Simulated degradation of lunar impact craters and a new method for age dating farside mare deposits

Robert A. Craddock[1]

Center for Earth and Planetary Studies, National Air and Space Museum, Smithsonian Institution, Washington, D.C.

Alan D. Howard

Department of Environmental Sciences, University of Virginia, Charlottesville

Abstract. With the advent of Clementine data it is now possible to determine the lithology and extent of geologic materials on the Moon, particularly the farside mare deposits. However, traditional crater counting techniques do not provide reliable age estimates of these materials owing to their small surface areas. To support such studies, we present a model for estimating their age by analyzing the morphometry of degraded craters 1-3 km in diameter. A photoclinometric model was adapted for use with monoscopic 0.750-µm ultraviolet-visible and high-resolution images where we extracted the topography of fresh craters. A two-dimensional computer model simulating linear diffusional creep was applied to fresh craters at a variety of diameters. The resulting profiles were then compared to photoclinometric profiles of degraded craters of known ages for calibration. Application of the resulting model to degraded craters in the mare deposit of the central Apollo basin (-36.5° latitude, 208.0° longitude) indicates that this material was emplaced during the early Imbrian period (~3.85 Ga). By calculating the amount of material eroded from each of the degraded craters observed in this unit, the average erosion rate is estimated to be $2.0 \pm 0.1 \times 10^{-7}$ mm/yr on the Moon since the Imbrian. The estimated amount of material eroded during any given period suggests that the erosion rate has decreased with time, implying that the flux of larger impactors has as well.

1. Introduction

The age and composition of lunar maria record the thermal history of the Moon. These basaltic materials cover 7×10^6 km^2, or roughly 17% of that planet's surface area [*Head*, 1976], most of which are concentrated on the nearside. While the nearside deposits were sampled by the Apollo and Luna missions and have been intensely studied by Earth-based telescopic observations, the farside deposits have remained enigmatic. Apollo-era spacecraft focused on understanding the geology of the nearside, primarily in support of the manned missions. Thus farside mare deposits were poorly imaged with little or no remote-sensing data to derive their compositions. Now, however, global multispectral data obtained by the Clementine spacecraft make it possible to deconvolve the geology of the farside mare deposits. Unfortunately, several problems remain in age dating these lithologic units. Most individual emplacement units are areally small, so crater population data become statistically unreliable. In addition, the resolution of the Clementine ultraviolet-visible (UVVIS) camera is ~200 m/pixel on average [*Nozette et al.*, 1994], which makes craters <1 km in diameter difficult to recognize (Figure 1a). Images obtained by the Clementine high-resolution (HiRes) camera alleviate this problem, but the spatial coverage of these data is poor (Figure 1b), and again age dates based on crater populations become unreliable.

To assist in determining the ages of the units composing the farside mare deposits, we developed a technique that qualitatively assesses the amount of degradation that has occurred on individual craters 1-3 km in diameter through time. The results presented here show how the photometric function was derived so topographic information could be extracted from single, monoscopic Clementine images. From these data the profiles of degraded craters located in geologic units of known ages were analyzed to relate the crater diameter and the extent of degradation to lunar time-stratigraphic periods. On the basis of these observations, computer models simulating crater degradation (linear diffusional creep) on fresh crater profiles were performed to quantatively explore how the related flux of micrometeorite bombardment may have changed through time. Our results suggest that the impact flux has steadily decreased since the Imbrian, contradicting evidence that it has increased during the Copernican [*McEwen et al.*, 1997]. The computer simulations resulted in crater profiles that could be used as templates for determining the age of individual craters within any individual mare flow unit. Preliminary results from the analysis of degraded craters located in the central Apollo basin mare deposit indicates that this material is Imbrian in age (3.85-3.2 Ga).

2. Background

The most commonly accepted method for age dating geologic units on planetary surfaces is crater counting. Diameters of all the craters within a given unit are measured, and the cumulative number of craters at any given diameter is plotted on a log-log scale. For comparison to other units, the cumulative number of

[1]Also at Department of Environmental Sciences, University of Virginia, Charlottesville.
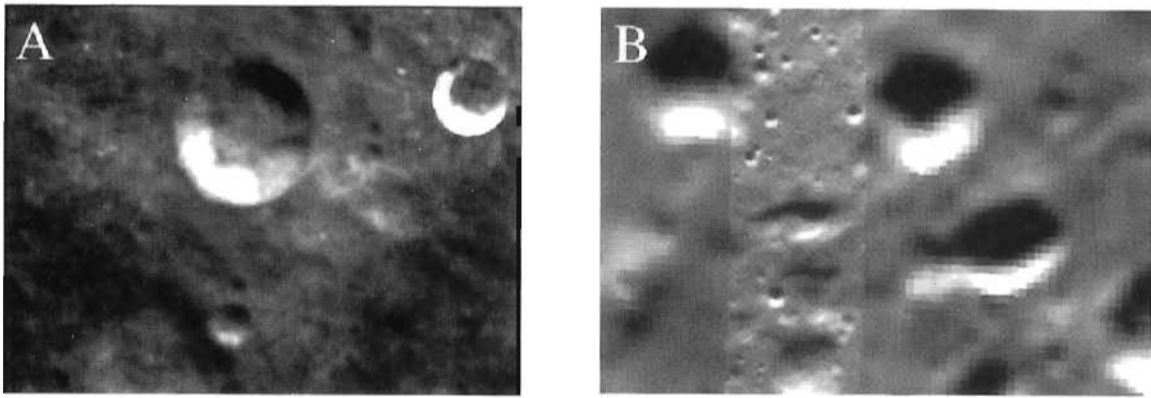
Figure 1. Lunar impact craters seen by the Clementine spacecraft: (a) a typical ultraviolet-visible (UVVIS) image (0.415-μm) which has a resolution of ~200 m/pixel and (b) a high resolution (HiRes) image superposed on a UVVIS image to compare the difference in resolution. The HiRes image is 2.9 km across and has a resolution sufficient enough to detect 1-m-sized objects on the surface. Note the lack of an obvious ejecta blanket associated with many of the craters in these images. Micrometeorite bombardment quickly degrades the color and surface texture of most lunar craters. Continued bombardment degrades and softens the general shape of the craters.

craters is generally normalized to some specified area (e.g., 10^6 km^2), and estimates of age are made either by measuring the slope of the curve(s) or by determining the cumulative number of craters at a certain diameter. For the Moon these values have been calibrated to absolute ages determined from returned samples (see discussion by *Wilhelms* [1987, pp. 121-136]). This technique, however, is subject to large errors when the areal extent of the geologic unit is small (e.g., Figure 2). During the Apollo era, scientists recognized the importance of creating a reliable age-dating technique that could be applied to astronaut-scale geologic units investigated at the landing sites. Several were developed that are still in use today. The simplest, qualitative method was originally presented by *Trask* [1969, 1971] and was subsequently modified slightly [*Offield and Pohn*, 1970; *Pohn and Offield*, 1970]. From Lunar Orbiter data, *Trask* [1969, 1971] observed the morphological differences between fresh and degraded craters. He correctly assumed that fresh craters undergo modification from small impactors, which cause erosion of the rim crest and infilling of the crater floor. Because there is proportionally less material to erode on smaller-diameter craters, he deduced that smaller-diameter craters would take less time to erode completely than larger-diameter craters. A template showing representative craters at given diameter and degrees of modification is used for age dating [see *Trask* , 1971] (Figure 3). The caveat is that in order to get reliable ages from this method, the largest diameter crater that is still visible must be identified within the geologic unit.

A more quantitative approach was first devised by *Soderblom* [1970a, b], who presented a theoretical model of crater erosion operating in an assumed steady state environment. Similar to *Trask*'s [1969, 1971] technique, the largest modified crater is sought. However, Soderblom reeognized the fact that the largest-diameter crater is not always easy to identify. On a given surface, craters slightly larger in diameter than the saturation diameter Cs, will be less obliterated. He found that typically such craters have interior slopes of 1° and their diameter D_L (in meters) can be related to the Cs diameter by the relation $D_L = 1.7Cs$ [*Soderblom and Lebofsky*, 1972]. Values of D_L can be determined by two separate techniques [*Soderblom and Lebofsky*, 1972; *Boyce et al.*, 1975], and their values are fairly reliable for mare units but are

not as reliable for units contained in the lunar highlands [*Wilhelms*, 1987, p. 133]. In addition, successful application of the D_L technique is conditional. Typically, it requires photographs limited to Sun-illumination angles between 8° and 30° [*Soderblom and Lebofsky*, 1972], and the sample area must be at least 100 km^2 for young surfaces and 1800 km^2 for highland surfaces [*Boyce et al.*, 1975].

Although these techniques remain important for placing small geologic units into a regional context from Apollo-era photographs, they are not directly applicable to many of the Clementine UVVIS images of the farside maria. Particularly problematic is the fact that the Sun-illumination angle in these areas is typically >30°, so a distinct crater morphology cannot be recognized. Use of the D_L techniques is also arduous in that it requires the investigator to examine all the craters within a given unit. Again, however, craters <1 km in diameter are difficult to recognize in UVVIS data because of the resolution, while coverage by the HiRes camera was not global.

2.1. Usefulness of Clementine Data

Fortuitously, Clementine images have a resolution which is well suited to characterizing the degree of crater modification in the size range most useful for dating surfaces. To explain: craters less than ~1 km erode so quickly that many older craters have not survived up to the present day. On the other hand, modification of craters larger than ~3 km is not always discernible, and only the very oldest craters show signs of degradation [*Trask*, 1971]. Estimating the small degree of erosion on these large craters is made even more difficult because multiple Clementine images are needed to see the complete crater, which is not conducive to making quantitative measurements of crater shape. However, craters 1-3 km in diameter could potentially survive through all of lunar history. Also, they typically have discernible amounts of erosion while being contained within a single Clementine image.

At the time the D_L techniques were developed, only shadow measurements were available for describing the crater geometry, and the morphometry of both fresh and degraded craters were idealized from these data. The morphometry of individual craters can now be extracted from the Clementine images using
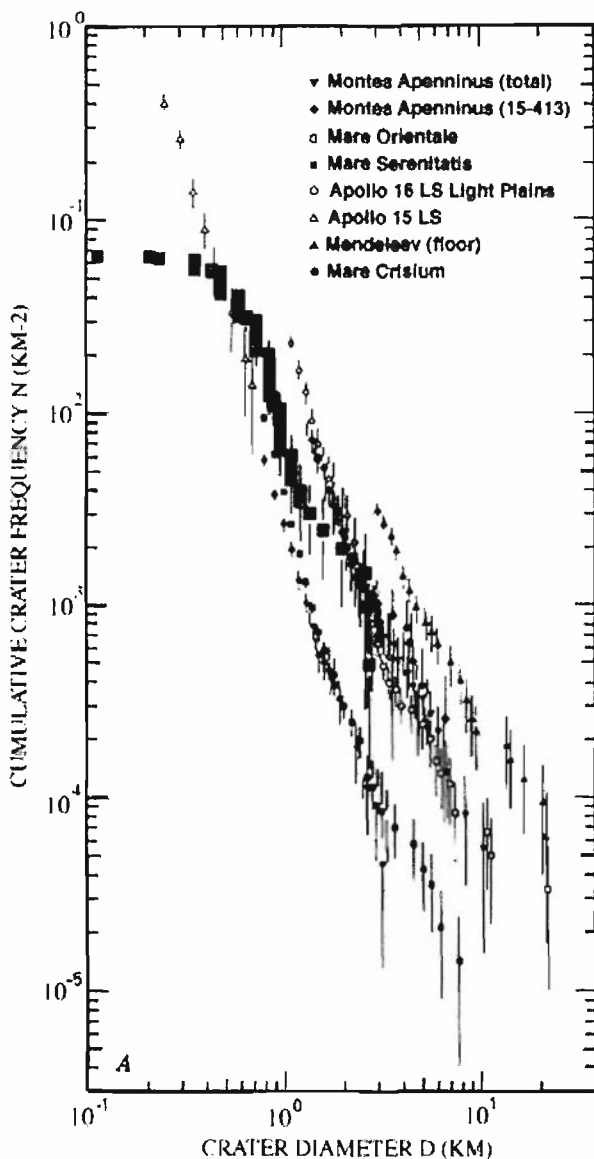
Figure 2. Crater frequency curve of the central Apollo basin mare deposit based on Clementine UVVIS data (large, solid squares) and compared to other sites on the Moon investigated with Apollo-era photographs. Note the "clumping" of data at specific crater diameters, which is an effect of UVVIS image resolution. The deviation from a simple power-law function makes comparison difficult. (Modified from *Wilhelms* [1987, Figure 11.2].)

based on the principle that variations in brightness values measured by a spacecraft's imaging system are directly related to the orientation of the surface element relative to both the Sun and the spacecraft. There are, however, several additional causes of brightness variations within an image other than topography. The sources for these variations in brightness can come from the detector itself (internal) or from a planet's surface properties or atmosphere (external).

Historically, an important source for internal, nontopographic brightness variations has been the detector itself (e.g., shading or "vignetting"). However, because the Clementine cameras were CCD instruments, such problems have virtually been eliminated. Other spacecraft sources of brightness variations that are potentially more problematic include coherent and random noise from the cameras as well as noise introduced into the images by telemetry problems or compression algorithms. Such inherent noises generally affect only relatively small portions of individual images and are easily identified. Calibration of raw Clementine images is performed in the planetary image processing program Integrated Software for Imaging Spectrometers (ISIS). The optical distortion on the UVVIS images is generally <1% geometrically, and these corrections can also be implemented in ISIS.

External sources for nontopographic brightness variations within an image come from a planet's atmosphere, surface scattering, and surface albedo variations. Atmospheric scattering is obviously not a factor in causing brightness variations in the Clementine imagery data, and surface scattering is minimal in expansive flat plains such as the lunar maria investigated in this
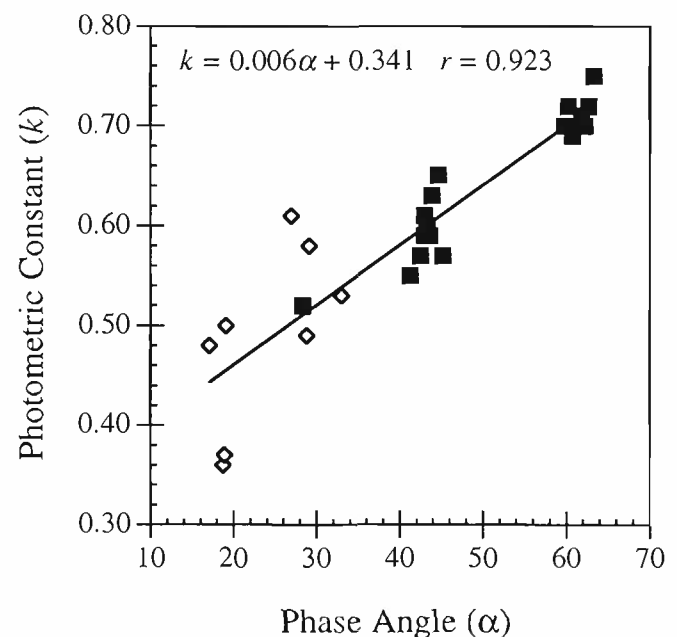

Figure 3. Value of the Minneart coefficient k as a function of phase angle α as applied to the 0.750-μm band pass filter on the Clementine UVVIS camera (and applicable to the HiRes camera). Values derived from Apollo stereophotogrammetric data (Lunar Topographic Orthophotomaps, LTOs) are shown as diamonds, and values derived from shadow height measurements are shown as squares. The scatter in the stereophotogrammetric results may indicate that height measurements made from these data are accurate only to within a few hundred meters.

photoclinometry, and these measurements can be used to determine how much erosion has taken place. Essentially, it is possible to derive a technique similar to those used to support Apollo-era investigations for age dating the mare units. To utilize the digital images obtained by Clementine, however, the two-profile photoclinometric model developed by *Davis and Soderblom* [1984] for use on martian craters imaged by the Viking orbiters had to be adapted first.

2.2. Photoclinometry and Applicable Photometric Function

Photoclinometry is a technique for obtaining topographic data from a single, monoscopic spacecraft image. This technique is

study. The image brightness in an individual pixel within a given Clementine image is thus the result of radiation reflected directly off the surface and into the spacecraft camera. Surface albedo variations, however, can present a serious problem in examining the lunar surface. Extreme variations in surface albedo, such as those typically associated with lunar dark halo craters, are especially difficult to deal with, and the safest method is to avoid them altogether. Slight albedo variations (i.e., a few digital numbers) can be accounted for using the symmetric photoclinometric method developed by *Davis and Soderblom* [1984], which is the method employed here and developed further below. (See discussions by *Davis and McEwen* [1984] and *Jankowski and Squyres* [1991] for additional information on the inherent errors in using photoclinometry.)

The intensity of radiation scattered from the surface into an imaging system is related to the intensity of the incident radiation that typically comes from a different direction. There are several mathematical expressions, or photometric functions, that allow investigators to calculate this relation. Ratioing two profiles in the symmetric photoclinometric method presented by *Davis and Soderblom* [1984] cancels out the effects of the intrinsic reflectivity of the surface, but this requires using the Minneart photometric equation which is expressed as:

$$I(\mu, \mu_0, \alpha) = B_0 \cos^k i \cos^{k-1} e \qquad (1a)$$

$$I(\mu, \mu_0, \alpha) = B_0(\alpha)\mu_0^{k(\alpha)}\mu^{k(\alpha)-1} \qquad (1b)$$

where $I(\mu, \mu_0, \alpha)$ is the reflective function (defined as the intensity of scattered light indicated by the cosine of the Sun-illumination angle μ, the cosine of the emission angle μ_0, and the phase angle α), B_0 is the surface normal albedo, i is the Sun-illumination angle, and e is the spacecraft emission angle. The Minneart coefficient k is a function of wavelength and increases directly with phase angle. A problem with the Minneart function is that it diverges toward infinity as emission angles approach 90°, so it is inappropriate to use with oblique viewing geometries. The Minneart coefficient k also does not offer a unique solution at low phase angles [*Goguen*, 1981]. However, *McEwen* [1991] observed that as the phase angle increased, the dependence of $I(\mu, \mu_0, \alpha)$ on the Minneart coefficient decreased and agreed well with values predicted by the third widely used photometric function, the Hapke function. Because the Hapke function [*Hapke*, 1981] appears to relate easily to the physical properties of surface materials and it has been applied successfully to a number of planetary surfaces, it is generally accepted as the definitive model for reflectance. However, its complexity makes it difficult for deriving photoclinometric measurements. The Hapke function has also produced poor results at high photometric latitudes [*McEwen et al.*, 1993, *Belton et al.*, 1994], which creates a potential problem when dealing with images taken near a planet's poles. Because it can be easily applied to the symmetric photoclinometric method, which is particularly useful in examining impact craters, the simplest analytical solution is the Minneart function. However, it will be applicable only to Clementine imagery data taken at phase angles >5°, which precludes using images taken at or near the equator because phase angle changes roughly as a function of latitude in Clementine data. Because a solution to the Minneart function does not exist for the spectral band passes utilized by the Clementine UVVIS and HiRes cameras, it was necessary to first derive one.

3. Crater Morphometry

3.1. Minneart Function

The Minneart coefficient k is wavelength dependent. Since the entire surface of the Moon was simultaneously imaged in six spectral band passes by the UVVIS camera [*Nozette et al.*, 1994], photoclinometric investigations require a Minneart function for at least one of these filters. We worked with images taken with the 0.750-µm UVVIS band-pass filter since they were some of the first fully calibrated data to be made available, an identical 0.750-µm filter flew on the HiRes camera, and 0.750-µm images are the best for investigating geologic features on the Moon.

We began by measuring impact craters located in the lunar maria that were also mapped on the Lunar Topographic Orthophotomaps (LTOs). Typically, the LTOs contain minimum and maximum elevation information about certain craters, which provide an estimate on the crater's depth. For individual profiles the Minneart coefficient was iteratively changed until the depth of the crater in the photoclinometric profile matched (or closely matched) the depth given on the LTO. Both the phase angle and the corresponding Minneart coefficient were then recorded. The LTOs provided a reliable control on determining the 0.750-µm Minneart function for craters located between 10° and 30° latitude, which corresponded to phase angles of ~17° and 35°, respectively. For craters located at higher latitudes, and thus imaged at correspondingly higher phase angles, crater depths were estimated using shadow measurements. The same iterative process for deriving the corresponding Minneart function was then performed using these measurements. In all, a total of 40 measurements were made at phase angles ranging from ~17° to ~62° (Figure 3). From these data the Minneart coefficient in the 0.750-µm band pass filter was found to be

$$k = 0.0060\alpha + 0.3412 \quad r = 0.923. \qquad (2)$$

It is interesting to note that estimates of k based on shadow height measurements tended to be more consistent than those derived from stereophotogrammetry (Figure 3). This suggests, perhaps, that the topography derived from Apollo Metric stereophotogrammetry has absolute errors of a few hundred meters (i.e., a few contour intervals).

3.2. Fresh Craters

On the basis of high resolution Lunar Orbiter and Apollo data, *Pike* [1974, 1977] determined the geometric relation between depth and diameter for 136 craters located in the lunar maria. Such measurements subsequently became the basis for numerous investigations, including estimates on the distribution of ejecta from impact craters [*McGetchin et al.*, 1973; *Settle et al.*, 1974]. These data also provide an important aid in understanding the cratering process itself [e.g., *Grieve et al.*, 1977]. In order to model the degradation of lunar impact craters, it is necessary to first understand the morphometry of the fresh craters. Also, because it was not possible to make reliable measurements of craters on the lunar farside prior to Clementine, it is necessary to compare populations of both nearside and farside impact craters to determine if they are morphometrically similar.

We defined fresh impact craters simply as those craters with bright (or high albedo) ejecta (Figure 4). As part of the degradational process, micrometeorite bombardment combined
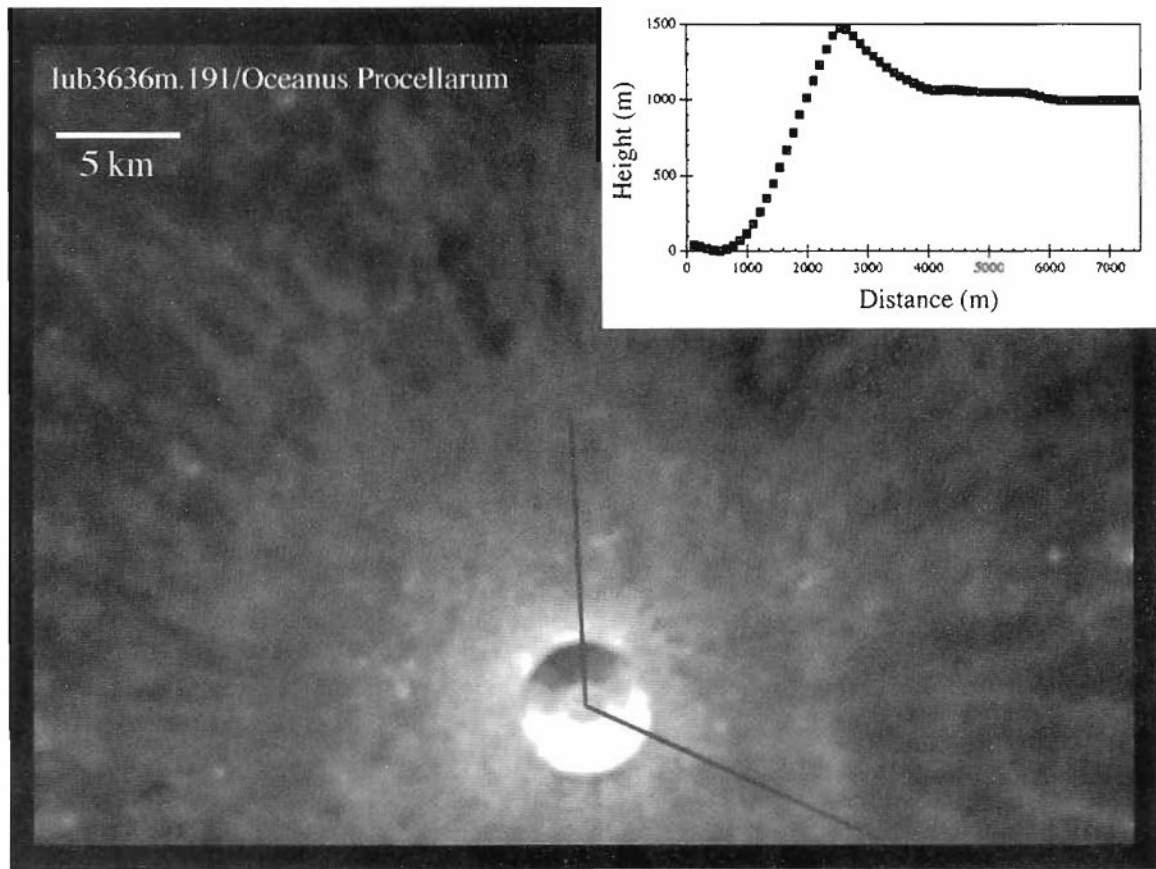
Figure 4. An example of a 5-km-diameter fresh lunar impact crater and its corresponding photoclinometric profile. Note the bright (i.e., high-albedo) ejecta blanket and a sharp, raised rim. These were the morphologic criteria used to denote fresh craters.

with high-energy solar and cosmic charged particles modify the upper few centimeters of the lunar soil in a process called maturation [*McKay et al.*, 1991]. As the upper few centimeters of crater ejecta matures, it becomes darker [e.g., *McEwen et al.*, 1993]. Although in some instances the amount of physical degradation is only minor, craters no longer retaining a bright ejecta deposit have obviously been modified and were thus avoided.

Fresh craters are often mistakenly referred to as "Copernican" craters in reference to the youngest geologic unit defined for the Moon. Copernicus is a 93-km-diameter impact crater located on the nearside and distinguished by its bright rays and sharp, rugged rim, which make it easily visible. It is estimated to have formed at <1 Ga [*Wilhelms*, 1987]; however, other impact structures have been forming during this period of time. Craters with diameters smaller than Copernicus would be modified more easily and thus would not maintain the morphologic characteristics typically associated with this crater (i.e., bright rays and sharp crater rim crests) even though in many instances they might be younger than Copernicus. For clarity, we define "fresh" as a crater sharing the same morphologic characteristics as the crater Copernicus; however, because many smaller, modified craters are Copernican in age, the terms "Copernican age" and "fresh" are not used synonymously.

Using the relationship described in (2), we made 35 photoclinometric measurements of fresh impact craters on the lunar nearside (Oceanus Procellarum, Mare Imbrium, Mare Figoris, and Mare Serenitatis) and 16 measurements on the lunar farside (Apollo, Tsiolkovsky, Jules Verne, and Moscoviense). Although measurements of fresh nearside craters represent a random sampling, the areal extent of farside maria is much less. As a result, the sampling of craters presented here is essentially the total population of fresh farside mare craters we were able to easily identify in the 0.750-μm Clementine images.

Of primary importance are crater depth and rim height versus crater diameter. The least-squares regression fit for crater depth versus diameter is best fit by a logarithmic curve described by the equation

$$d_F = 0.139 \ (\pm 0.054) D_F^{1.329 \ (\pm 0.246)} \quad r = 0.913, \qquad (3a)$$

where d_F is the fresh crater depth (km) measured from the lowest point in the crater to the maximum rim height and D_F is the fresh crater diameter (km) defined by the occurrence of maximum rim height. For comparison, *Pike* [1974] found values of 0.196 for the coefficient and 1.010 for the exponent (standard errors not expressed). Values for fresh nearside and farside craters were similar and can be described by the equations

Nearside $\qquad d_F = 0.155 D_F^{1.273} \quad r = 0.910,$ (3b)

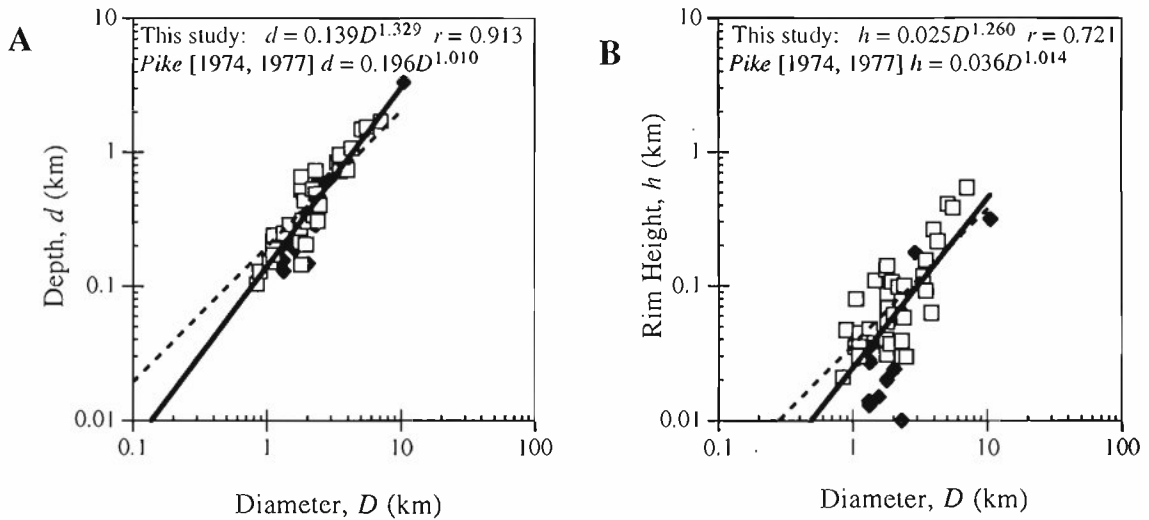Farside $\qquad d_F = 0.117 D_F^{1.398} \quad r = 0.931.$ (3c)

Figure 5. Morphometric relations of fresh lunar craters <10 km in diameter from both the lunar nearside (squares) and farside (diamonds): (a) crater depth versus diameter and (b) crater rim height versus diameter. Relations defined by *Pike* [1974, 1977] from Apollo stereophotogrammetric data are shown as dashed lines for comparison. Not surprisingly, these previously defined relations remain valid. However, there is more variability than *Pike*'s [1974, 1977] data suggest. These data support the Minneart function presented in Figure 3 (2).

For crater rim height, the least squares fit is described by

Total $h_F = 0.025 \ (\pm 0.064) \ D_F^{1.260 \ (\pm 0.076)} \quad r = 0.721$,   (4a)

Nearside $h_F = 0.033 D_F^{1.143} \quad r = 0.749$,   (4b)

Farside $h_F = 0.0.15 D_F^{1.347} \quad r = 0.745$,   (4c)

where h_F is the fresh crater rim height in kilometers measured from the maximum rim height to the precrater ground level. For comparison, *Pike* [1974] found values of 0.036 for the coefficient and 1.014 for the exponent (standard errors not expressed). Not unexpectedly, nearside and farside craters are morphometrically identical to one another and can essentially be described by *Pike*'s [1974] equations (Figure 5). These data also support the reliability of the Minneart function expressed in (2). Knowing the fresh crater profiles, it is now possible to derive degraded profiles to use for age dating.

3.3. Two-Dimensional Simulations of Crater Degradation

The photoelinometrically derived fresh crater morphometry was assumed to be representative of all fresh craters that formed on the mare surfaces through time. Using the drainage evolution model presented by *Howard* [1994] and applied to martian impact craters by *Craddock et al.* [1997], we simulated lunar crater degradation in cross section and expressed the rate laws in cylindrical coordinates. Although *Howard* [1994] distinguished between advective (scale-efficient) and diffusive (scale-inefficient) processes, only the latter need be used to describe lunar crater degradation [*Soderblom and Lebofsky*, 1972; *Boyce and Dial*, 1975]. Diffusional processes smooth and round the landscape and are distinguished from advective processes in that they require steeper gradients with increasing contributing area under steady state conditions.

From the *Howard* [1994] model, diffusive (or mass-wasting) processes, $\partial z / \partial t|_m$, are expressed as the spatial divergence of the vector rate of movement

$$\partial z / \partial t|_m = -Ks \nabla \bullet S, \qquad (5)$$

where S is the vector of slope gradient and the constant Ks is assumed to be spatially and temporally invariant. In each of the simulations the amount of material eroded during an individual event was assumed to be small in comparison to the scale of the crater, so that degradation can be approximated as being continuous. In each simulation the resulting modification was measured over fixed time intervals to assess the process and scale efficiency. Also, only simple linear diffusional creep was considered, meaning that slopes in our simulations never reached an angle where materials would then slump catastrophically. This assumption is true of most craters <15 km in diameter [e.g., *Smith and Sanchez*, 1973].

Our goal was to create a variety of simulated profiles that matched degraded crater profiles of known absolute ages. Such profiles could then function as digital representations of the craters used in the *Trask* [1971] template. This is needed because the emphasis of the Clementine mission was in obtaining multispectral images [*Nozette et al.*, 1994], and so the "time of day" (i.e., the Sun-illumination angle) was frequently not favorable for making morphologic observations. It is therefore difficult to recognize subtle variations in crater morphology, particularly at lower to midlatitudes, where the Sun is more directly overhead. Once calibrated, these profiles are useful in estimating age dates of materials and individual craters. Also, because the simulated profiles are collected at fixed time intervals, they are more useful in estimating temporal variations in the rate of erosion and the scale dependency of this process.

3.3.1. Calibration. From Figure 6 it is clear that crater diameters between 1 and 3 km are the most useful in relative age dating the widest range of geologic periods (Imbrian to the Copernican, 3.85 Ga to the present; Table 1). The simulations show that craters smaller than 1 km are destroyed if they are older than the Eratosthenian period, and craters larger than ~5 km are not heavily modified even if they are Imbrian in age. While this observation was made well before the Apollo era [e.g., *Trask*,
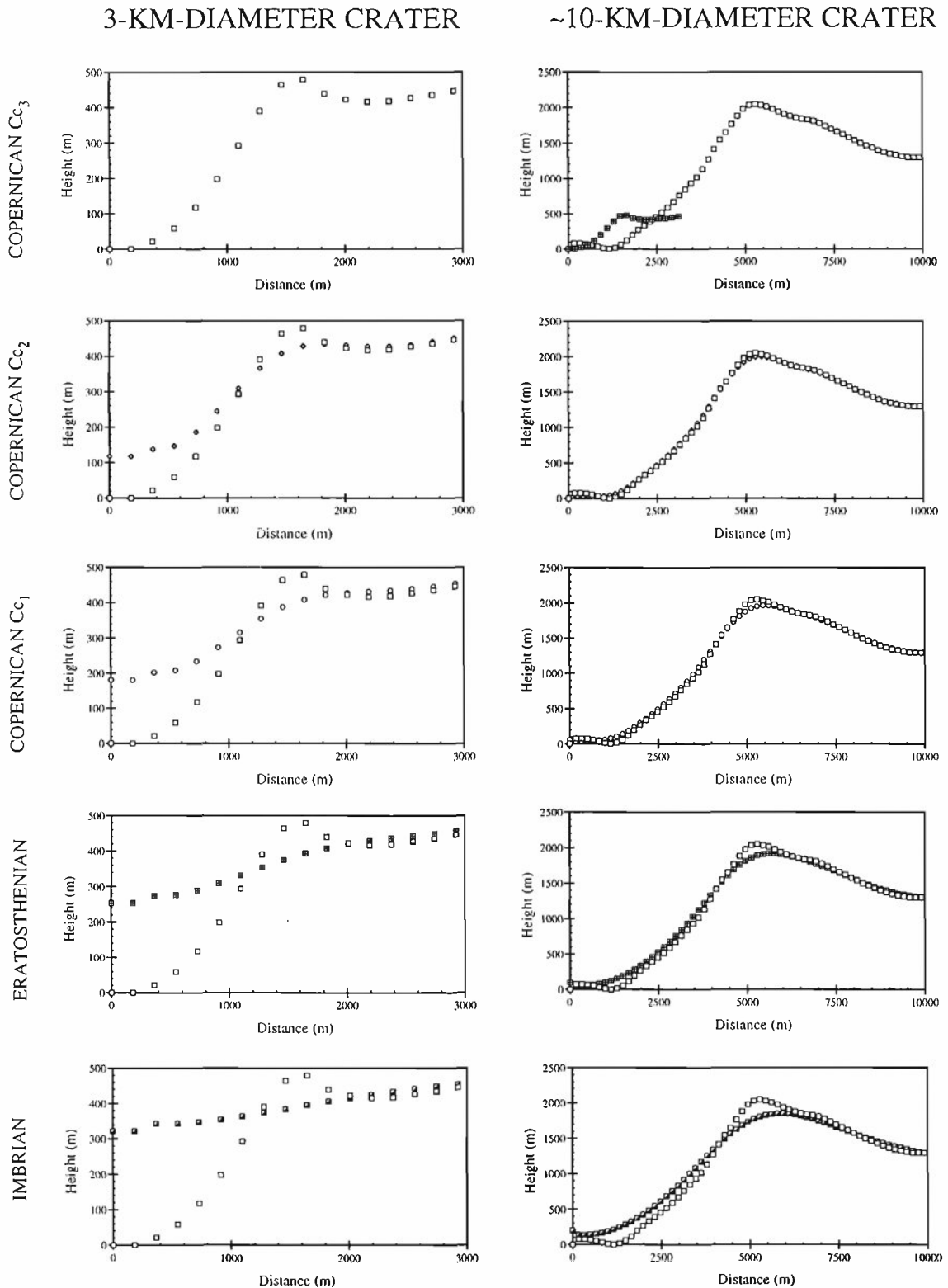
3-KM-DIAMETER CRATER   ~10-KM-DIAMETER CRATER

Figure 6. Two-dimensional simulations of lunar crater degradation. The fresh crater (solid squares) is shown in each step for comparison. In these simulations the left-hand boundary is free to move vertically, but no material is transported beyond this point. The right-hand boundary is fixed at the initial elevation, and mass is conserved in the erater interior but may exit the system to the right. The curves presented for a 3-km-diameter crater (left) were calibrated to craters within the vicinity of the Apollo 15 landing site. The 10-km-diameter crater (right) was subjected to the same rate-governing parameters and total time of simulation as the smaller crater on the left. (The smaller crater is also shown at the same scale as the larger counterpart in the upper right diagram.) Craters 1-3 km in diameter (left) are useful in age dating the widest range of geologic material on the Moon [*Trask*, 1971], are more common than larger diameter craters [e.g., *Wilhelms et al.*, 1978], and are easily resolved within individual Clementine UVVIS frames.

Table 1. Lunar Stratigraphic Systems

System	Typical Units	Age, Ga
Copernican	fresh, rayed craters, minor maria	(1.1) 2.1[a] - present
Eratosthenian	slightly degraded craters, significant maria	3.2 - 2.1[a] (1.1)
Imbrian	Imbrium and Orientale basins; Cayley Plains; degraded craters; most maria	3.85 - 3.2
Nectarian	Nectaris and 12 other basins; many degraded craters; some light plains	3.85 - 3.92
Pre-Nectarian	basins and craters; volcanic and intrusive igneous rocks; megaregolith and crust	before 3.92

[a]Calibration of the Copernican/Eratosthenian boundary based on shocked Apollo 15 KREEP samples [*Ryder et al.*, 1991]. Ages presented in parentheses are from *Wilhelms* [1984].

1971], these simulations validate the focus on craters 1-3 km in diameter for deriving our crater degradation model.

Despite the fact that six manned Apollo missions successfully returned samples from the Moon's surface, safety requirements and engineering constraints required that the Lunar Module land near the equator [see *Brooks et al.*, 1979; *Wilhelms*, 1993, and discussions therein]. Because of their location, most of these landing sites were imaged by the Clementine spacecraft at phase angles <5°, which is unsuitable for photoclinometric investigations [*Goguen*, 1981]. Fortunately, however, Apollo 15 landed at a latitude >26° and in basaltic material upper Imbrian in age [*Swann et al.*, 1972]. These basalts have $^{87}Rb/^{86}Sr$ and $^{87}Sr/^{86}Sr$ ages of ~3.3±0.1 Ga [*Compston et al.*, 1972; *Taylor*, 1982, Table 6.6], and the geologic unit they compose extends well into the Imbrium basin [*Carr et al.*, 1971; *Howard et al.*, 1972], which provides an excellent sampling area for calibrating our crater degradation model. Near the Apollo 15 landing site itself, many less degraded, and presumably younger craters were already assigned Copernican ages on the basis of Apollo-era D_L estimates (Plate 1a). These craters were also analyzed to provide a means for calibrating our model.

We derived photoclinometric profiles of craters 1-3 km in diameter within the geologic unit(s) presented in Plate 1 and then compared these measurements to profiles derived in our computer simulations. The most degraded craters were assumed to be the oldest and were assigned an Imbrian age. Copernican craters at various stages of degradation and preassigned a D_L age were extremely useful in calibrating the model curves. In every instance it was apparent that the crater shapes extracted through photoclinometry reflected the values assigned to them during the Apollo era [*Howard et al.*, 1972].

The absolute age dates derived for the lunar periods (and our modeled crater profiles) are based on Apollo samples [*Compston et al.*, 1972; *Taylor*, 1982, Table 6.6; *Ryder et al.*, 1991] , cratering frequencies for the extended calibration geologic unit presented in Plate 1 [*Neukum et al.*, 1975], and D_L estimates made around the Apollo 15 landing site [*Carr et al.*, 1971; *Howard et al.*, 1972; *Moore et al.*, 1980a, b]. Unfortunately, the absolute ages of the lunar periods has become somewhat controversial following the Apollo missions. While an age of ~3.3 Ga corresponds well to those craters that have undergone degradation

since the Imbrian, the time marking the beginning of the Copernican period is unclear. Age dates of Apollo 15 KREEP (i.e., high K, rare earth element, P, and other trace elements) basalt samples indicate that a major impact event shocked three of the returned samples at 2.1 Gyr ago. Because these samples were returned from a ray of an early Copernican age crater, Autolycus, *Ryder et al.* [1991] used the age date of the shock event to estimate the age of this crater and establish an alternative date for the Copernican period. However, it appears that many craters in the lunar maria have been misdated [*McEwen et al.*, 1997], primarily because they occur on low-albedo materials and thus often look fresh (i.e., have "bright" ejecta) in visible band passes [*Lucey et al.*, 1995, this issue]. Multispectral analyses of these craters indicates that their ejecta is too mature to be Copernican in age, and Autolycus may actually be an Eratosthenian age crater (A. McEwen, personal communication, 1998). For completeness, absolute ages presented by *Wilhelms* [1984] and *Ryder et al.* [1991] are presented (Table 1).

3.3.2. Age-dating application. Because impact craters form continuously after the deposition of a geologic unit, most will have a degradation age that is younger than the actual age of the unit. The minimum age estimate of the unit is represented by the most degraded crater. Analyses of degraded impact craters within Mare Imbrium show this effect. While most craters are Copernican or Eratosthenian in age, a few craters indicate that this unit was emplaced during the late Imbrian period, ~3.3 Ga. Before proceeding to age date the farside mare deposits, it was important to develop an understanding as to how useful (or robust) the model crater profiles are. As a test of their accuracy, we derived photoclinometric profiles of degraded impact craters in the Lambert (LTO40A3) and McDonald (LTO40A2) quadrangles, which contain a mare unit that is Eratosthenian in age (Plate 1b). The most degraded craters examined closely matched the model profile of an Eratosthenian age crater (Figure 7), which agrees well with the age determined by conventional geologic mapping techniques [*Wilhelms and McCauley*, 1971].

This test provided confidence to begin applying this technique to the mare deposits on the lunar farside, and results from the Apollo basin are presented here. Mare material in the central Apollo basin (-36.5° latitude, 208.0° longitude) covers only 1929
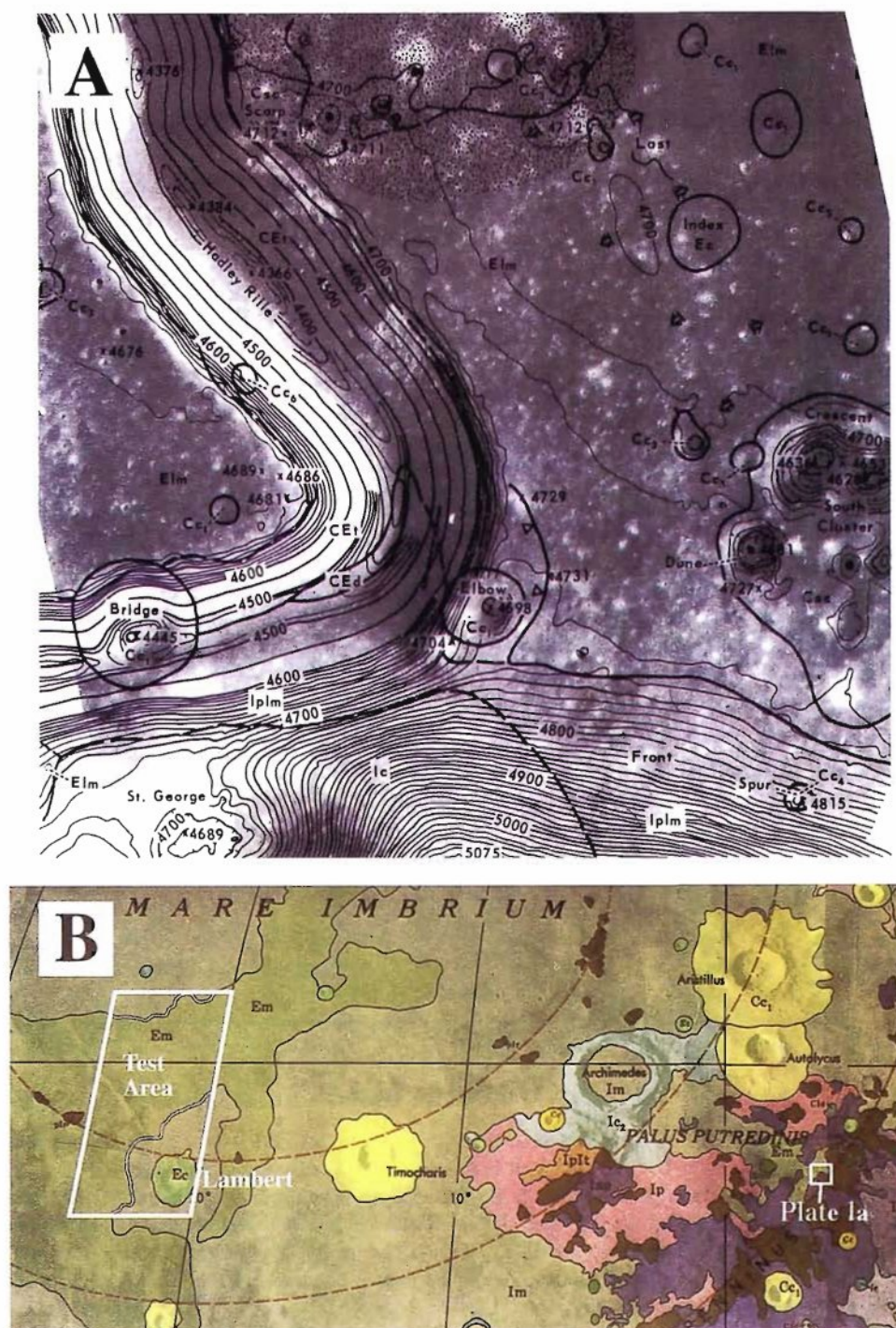
Plate 1. Geologic maps of Mare Imbrium around the Apollo 15 landing site showing the location of the Eratosthenian/Imbrian age mare deposit (Elm/Em) used to calibrate our model. (a) Apollo 15 landing site geologic map derived from orbital images and astronaut traverses. Note the occurrence of Copernican age craters (Cc_1, Cc_2, and Cc_3), which were dated by *Swann et al.* [1972] using the D_L technique. These craters and others on the *Carr et al.* [1971] map (not shown) were used, in part, to help calibrate our model. (b) Nearside geologic map showing a portion of the Imbrium basin which places the landing site map into a regional context [*Wilhelms and McCauley*, 1971]. Note the location of Eratosthenian age materials (Em), which is the location of the Lambert (LTO40A3) and McDonald (LTO40A2) quadrangles (box) where photoclinometric measurements of degraded craters were made to test the accuracy of the degradation model.
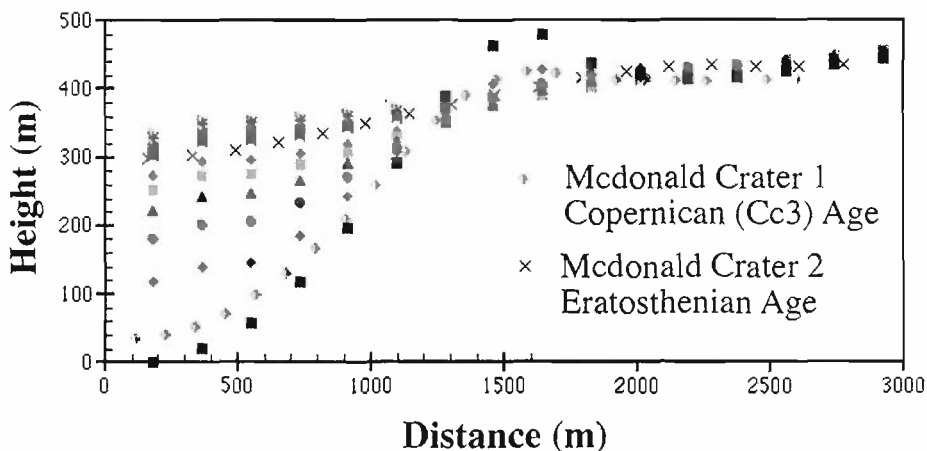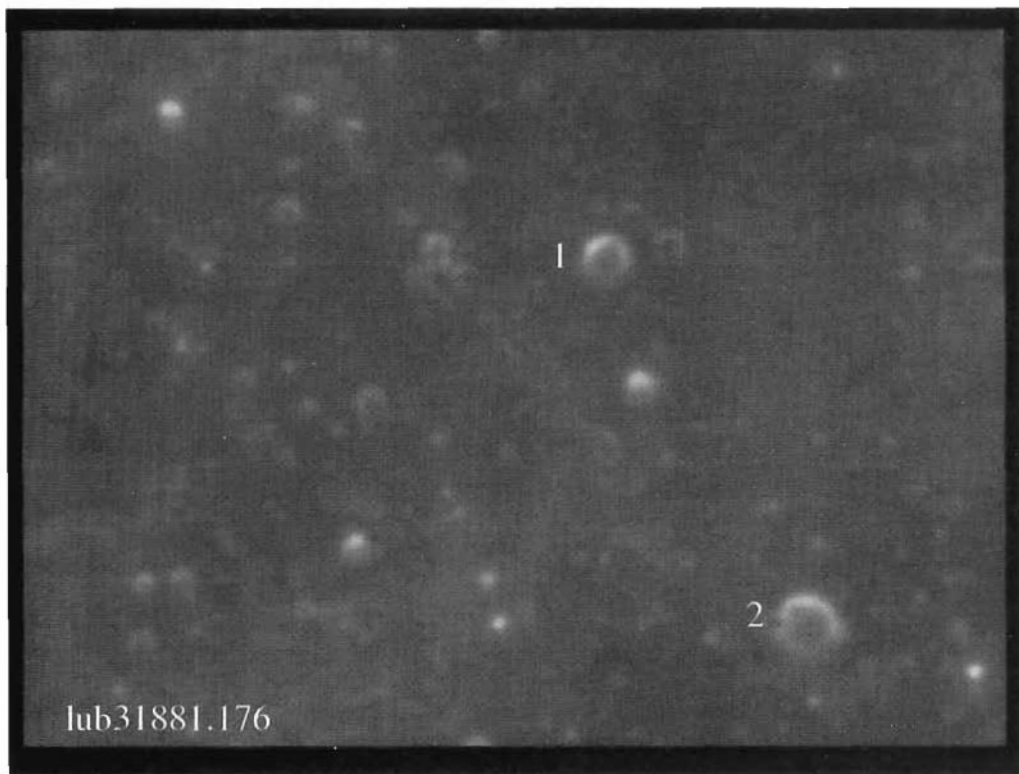
Figure 7. Clementine frame LUB31881.176 showing one of the oldest craters identified in the McDonald quadrangle (LTO40A2), indicating that the mare unit in this region (test area shown in Plate 1) is Eratosthenian in age. A Copernican age (Cc_3) crater is also visible in the same frame. The symbols to the model crater curves are the same as those presented in Figure 6. The Sun-illumination angle in this image does not make simple visual classification of a crater's degradation state possible. Because Clementine was designed to obtain multispectral data [*Nozette et al.*, 1994], the Sun-illumination angle in most images obtained at lower latitudes is typically poor for identifying subtle differences in morphology.

km^2 (Figure 8). Interestingly, this material is located at one of the topographically lowest points on the lunar surface [*Zuber et al.*, 1994]. Presumably, the South Pole-Aitken basin, the largest (2500 km) and deepest (8.2 km below the reference ellipse) impact basin in the Solar System [*Zuber et al.*, 1994], formed early in lunar history. Subsequently, the Apollo basin formed, excavating even deeper into the crust.

The diameters of craters identified in 0.750-µm UVVIS images were measured and counted, resulting in a crater frequency (larger than 1 km in diameter per square kilometer) of $6.6(\pm1.9)\times10^{-3}$ (Figure 2). This crater frequency is less than the age of the mare deposit at the Apollo 17 landing site (9.0×10^{-3}; early Imbrium [*Neukum et al.*, 1975], but substantially older than any of the other mare deposits investigated by the Apollo astronauts [*Wilhelms*, 1984]. However, comparison of the Apollo mare crater frequency curve to those determined for other units is difficult to make (Figure 2). The variation in the slope of the Apollo mare curve may reflect crater burial during mare
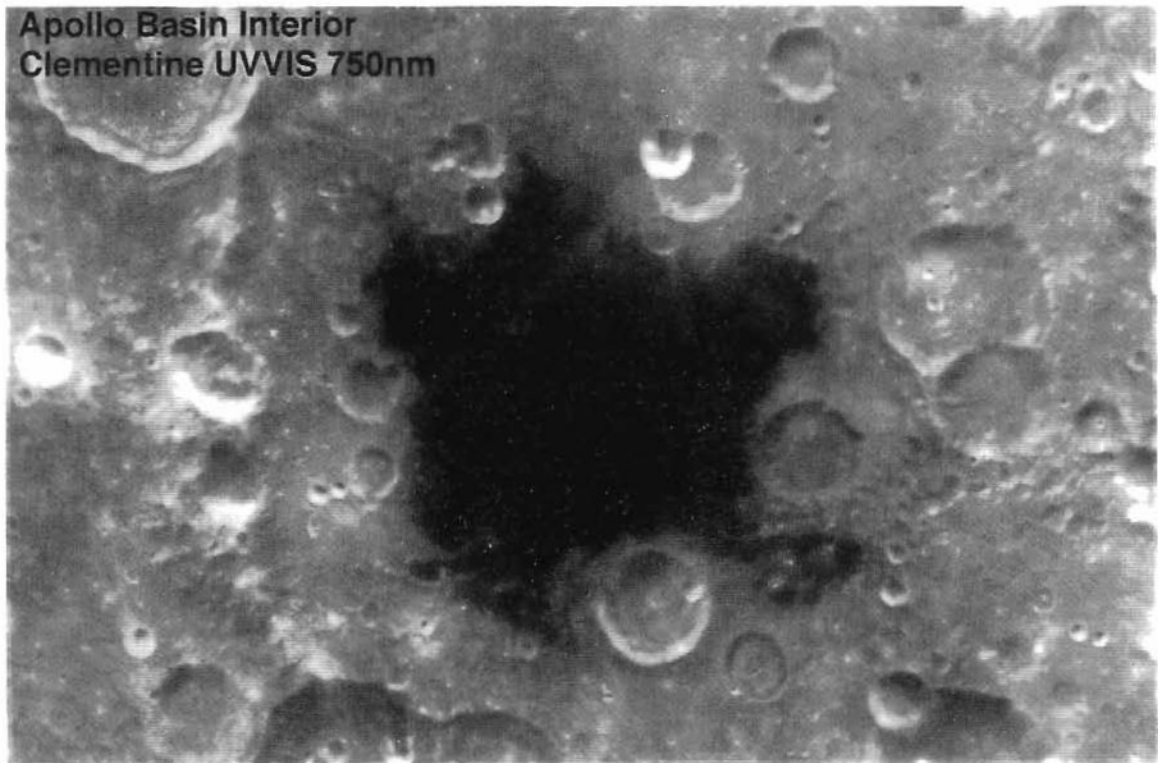
Figure 8. Clementine 0.750-μm UVVIS photomosaic of the mare located in the central Apollo basin (-36.5° latitude, 208.0° longitude). Examination of this photomosaic indicates the mare covers 1929 km². Interestingly, this deposit is located at the topographically lowest points on the lunar surface [*Zuber et al.*, 1994].

emplacement or it may be influenced by the resolution of the images analyzed (115 or 207 m/pixel). Analysis of degraded crater morphometry is an obvious way to verify these results.

Our model was applied to the eight degraded craters in the Apollo mare deposit with diameters >1 km. The most degraded ~1-km-diameter crater had a morphometry comparable to Imbrian age craters (Figure 9). The other craters (not shown) had morphometries consistent with younger age craters (Eratosthenian to Copernican). This result emphasizes the need to examine all craters within a geologic unit as the most degraded craters are the best indicators of geologic age. Because the oldest age is based on only one degraded crater in the example
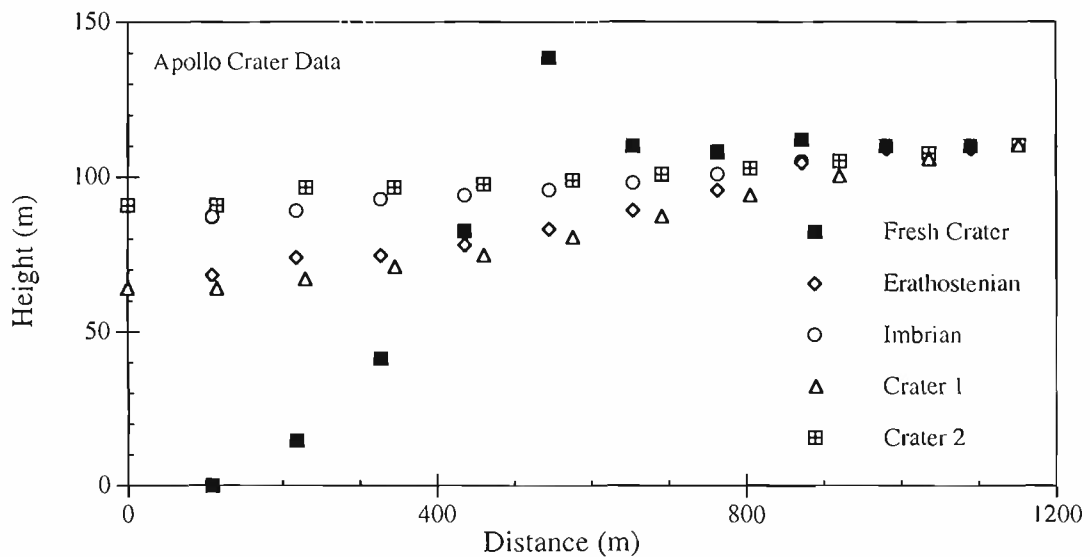

Figure 9. Degraded ~1-km-diameter craters within the centeral Apollo mare deposit. The oldest crater observed in the deposit was Imbrian in age (crossed squares), which corresponds to the crater frequency age. Accurate age determination of geologic units based on degraded crater morphometry is predicated on examining all the observed degraded craters within the unit.

presented here, our model obviously does not eliminate the need for other traditional age-dating techniques such as crater frequency curves. However, it is a suitable replacement for the various D_L techniques, which are not directly applicable to the Clementine images. Although the morphometry of the degraded craters in the Apollo mare concurs with the unit age determined by the crater frequency (i.e., Imbrium), it does supply an independent verification and suggests that the mare deposit in the Apollo basin may be one of the oldest on the Moon.

4. Rate of Erosion

Radiometric age dates for a variety of geologic units on the Moon have been made using the samples collected by the Apollo astronauts. The most highly degraded craters within these units allow an estimate of the lunar erosion rate to be made, which in turn implies what the micrometeorite flux rate may have been through time and how it may have changed. In addition, estimates of the erosion rates for the Earth [e.g., *Fournier*, 1960] as well as for Mars [*Craddock et al.*, 1997] have been made, and an estimate of the lunar erosion rate would make for an interesting comparison. Although a variety of "erosion rate" estimates already exist, these were used to understand the emplacement history of rocks collected by the astronauts [*Gault et al.*, 1972; *Hörz et al.*, 1991] or the waxing and waning of regolith thickness due to large impact craters [e.g., *Langevin and Arnold*, 1977]. Essentially, by looking at the degradation of large surface features (i.e., impact craters), the erosion rate estimate presented here is more comparable to the traditional definition.

Photoclinometric profiles of the degraded craters in the Apollo mare deposit were plotted and fitted with polynomial equations to describe their shapes (Figure 10). To avoid using higher order polynomial equations (which were more complicated to integrate and did not improve the correlation), the referent fresh craters (1, 2, and 3 km in diameter) were fitted with two separate equations. The first equation

$$y = -2.393 \times 10^{-10}x^4 + 5.484 \times 10^{-7}x^3 - 9.656 \times 10^{-5}x^2$$
$$+3.312 \times 10^{-2}x - 1.705 \quad r = 0.999, \tag{6}$$

describes the interior shape of the fresh crater up to the rim crest. The second equation

$$y = 7.099 \times 10^{-11}x^4 - 7.511 \times 10^{-7}x^3 + 3.007 \times 10^{-3}x^2 - 5.350x$$
$$+ 3965 \quad r = 0.994, \tag{7}$$

describes the exterior shape of the fresh crater from the rim crest out to the edge of the ejecta. A ~3.3 Ga degraded Imbrian age crater is shown in Figure 10 for comparison. Its shape can be described by the equation

$$y = -7.937 \times 10^{-9}x^3 + 4.267 \times 10^{-5}x^2 - 1.846 \times 10^{-2}x + 343.7$$
$$r = 0.999. \tag{8}$$

The combination of the fresh and degraded crater shape equations describes four separate portions which represent areas of net erosion or deposition. Eroded and infilled volumes were estimated by the determining the cross-sectional area (Figure 10) through integral calculus, determining the centroids of these area, and then using the theorem of Papus, or

$$V = (2\pi b)(A) \tag{9}$$

where b is the radius of the centroid and A is the area. The baseline for determining the differences between the crater profiles was the precrater ground height in meters (i.e., the total depth of the crater minus the crater rim height). The total estimated volume of modified material was then divided by the surface area of the crater out to the edge of the continuous ejecta deposit. Although it is likely the degraded craters measured in the Apollo basin mare deposit were not exactly 1, 2, or 3 km in diameter when they were fresh, the referent craters provided a decent approximation (e.g., Figure 2).
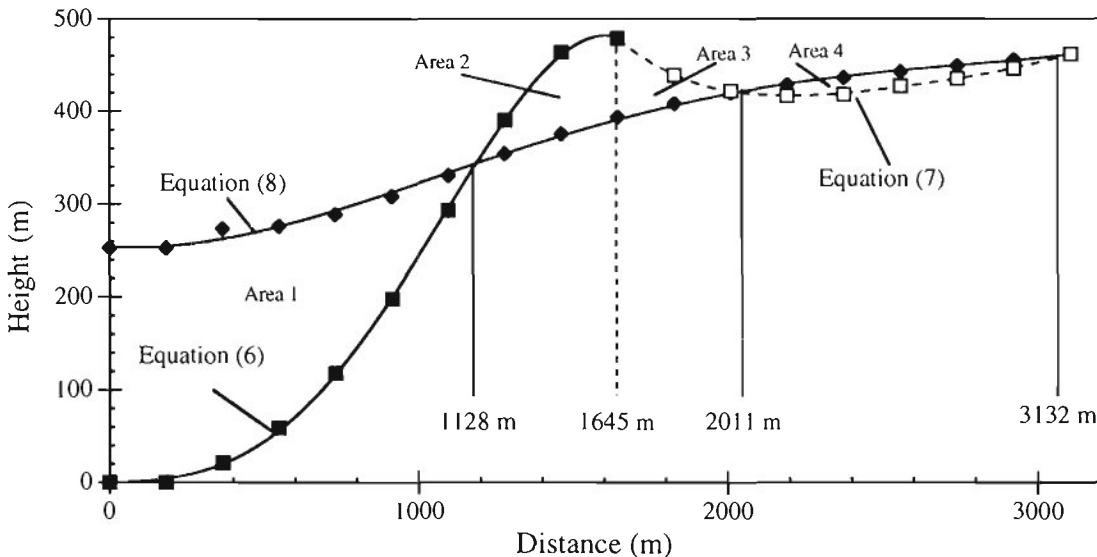

Figure 10. A schematic diagram of a fresh and a degraded Imbrian age 3-km-diameter impact crater showing the measurements used to calculate the amount of erosion that has taken place on the Moon. In this example the fresh crater rim is 1645 m from the center as indicated by a dashed line. Equation (6) describes the interior shape of the fresh crater up to the crater rim crest, and equation (7) describes the exterior shape. The solid lines denote values of x (i.e., the distance in meters) where values of y are the same for both the fresh and degraded crater. These values were used to integrate for each of the four eroded or depositional areas.

The total estimated volume of material eroded in the Apollo mare deposit is 1.8 km^3. When divided by the surface area (1929 km^2), the effective thickness of material modified is ~1 m (0.93 m). The rate of erosion was determined by dividing this value by the absolute age of the Imbrian period given in Table 1. From these data the average erosion rate from the Imbrium period is 2.0±0.1 x 10^{-7} mm/yr or, in terrestrial terms, 0.0002 Bubnoff units (B). (The errors reflect the estimated errors for the radiometric age dates of the Apollo samples [*Wilhelms*, 1984; *Ryder et al.*, 1991].) Because the age of the mare deposit in Apollo appears to be one of the oldest on the planet, which is supported by both crater frequency estimates and crater morphometry, this erosion rate essentially represents an average throughout most of lunar history. By comparison, erosion rates on early Mars were ~0.0003 [*Craddock et al.*, 1997] to 0.004 mm/yr [*Craddock*, 1999], and values in Virginia are ~0.004-0.2 mm/yr [*Fournier*, 1960]. Erosion rates on the Moon are several orders of magnitude less than those estimated for the other terrestrial planets. Analyses of degraded craters within other maria emplaced at different ages may help determine how the lunar erosion rate changed with time, which would indicate variations in the micrometeorite (~1-mm particle size) impact flux rate. However, the computer simulations of lunar crater degradation can provide a relative approximation.

5. Temporal Variability

There is some indication from the cratering record suggesting that the lunar erosion rate may have fluctuated through time. Because the Eratosthenian was a shorter interval of time (1.1 Gyr) than the Copernican (2.1 Gyr) [*Ryder et al.*, 1991], and it contains twice as many craters >30 km in diameter (88 compared to 44) [*Wilhelms*, 1987], *Ryder et al.* [1991] suggested that the average cratering rate preceding the Eratosthenian was twice as great. However, Clementine data provide a more accurate assessment of the number of impact craters that are Copernican in age. Because of its global coverage at low phase angles and the multispectral capabilities of the UVVIS camera, bright-rayed craters are particularly easy to identify [*McEwen et al.*, 1997]. Previously, bright ray craters contained in the nearside mare deposits were mapped as Copernican in age, but a multispectral assessment of the soil maturity of many of these craters using the *Lucey et al.* [1995] model suggests that they are Eratosthenian. Essentially the rays to these craters are still visible because they stand out in contrast to the darker, underlying mare deposit [*McEwen et al.*, 1997]. After correcting for the misidentified bright-rayed craters on the nearside and counting the previously unidentified bright rayed craters on the farside, *McEwen et al.*

[1997] determined that the average cratering rate during the Copernican was actually ~35% greater than the Eratosthenian. *Weissman* [1990] suggested that encounters with distant stars would periodically perturb cometary objects contained in the Oort Cloud approximately every 300-500 Myr, thus causing intense comet showers within the Solar System. If the cratering rates were higher during the Copernican, it follows that the flux of smaller objects responsible for crater degradation should also be higher during the Copernican. Our computer simulations provide a way of testing this hypothesis.

The calibrated curves presented in Figure 6 provide information on the relative rates of erosion during each lunar time stratigraphic period (Table 1). In each of our computer simulations, lunar crater degradation was modeled as being steady through time. At fixed intervals, x and y values describing the modified crater shape were written into a file for analysis later. The resulting profiles were then plotted and compared to crater profiles of known (or suspected) geologic ages. It is these profiles that are presented in Figure 4. However, because the sampling interval was fixed, many of the profiles occurring between calibrated curves are not shown. The relative rate of lunar erosion through time can be determined by comparing the number of intervals separating each of the calibrated profiles to their related ages (Table 2).

From Table 2 it appears that lunar erosion has decreased since the Imbrian. If the model chronology presented by *Ryder et al.* [1991] is correct, then lunar erosion has been decreasing almost exponentially through time. Alternatively, if the model chronology presented by *Wilhelms* [1984] is correct, then lunar erosion decreased sharply following the Imbrian and has remained fairly uniform since. Regardless, if the micrometeorite bombardment on the Moon is reflective of the flux of larger impacting objects (meters to kilometers in diameter), these estimates do not support an increase in the cratering rate during the Copernican as suggested by *McEwen et al.* [1997].

6. Conclusions

For the first time, Clementine data has allowed a digital assessment of the morphology of fresh lunar impact craters to be made. Not unexpectedly, fresh craters on the lunar farside are morphometrically identical to craters on the nearside. The geometric relations for fresh impact crater characteristics defined by *Pike* [1974, 1977] remain valid; however, there appears to be more variability in these relations than his data would suggest. Morphometric measurements of the fresh impact craters also support the Minneart function determined for the 0.750-μm band pass filters for the UVVIS and HiRes cameras (2). This relation

Table 2. Relative Rates of Lunar Erosion

System	Age, Ga[a]	Time, Gyr	Intervals	Intervals per 10^9 Years
Copernican	2.1[b] (1.1) - present	2.1 (1.1)	2	0.95 (1.82)
Eratosthenian	3.2 - 2.1[b] (1.1)	1.1 (2.1)	4	3.63 (1.90)
Imbrian	3.85 - 3.2	0.65	8	12.3

[a]From *Wilhelms* [1984].
[b]Calibration of the Copernican/Eratosthenian boundary based on shocked Apollo 15 KREEP samples [*Ryder et al.*, 1991]. Ages and time presented in parentheses are from *Wilhelms* [1984] and are shown for comparison.

will support future photoclinometric measurements using the *Davis and Soderblom* [1984] model.

Age dates of geologic units identified through the multispectral capabilities of the Clementine spacecraft are difficult to obtain. Many of these units are not extensive, so traditional crater-counting techniques do not provide meaningful statistics. Also, because the emphasis of the Clementine mission was on obtaining multispectral data, the Sun-illumination angle in images was typically high, particularly at low to midlatitudes, where most of the mare deposits are located on the Moon. Typically, it is difficult to recognize subtle variations in crater morphology, so traditional relative age-dating techniques, such as the D_L method, are not applicable the Clementine data. Using the diffusion model of *Howard* [1994], two-dimensional simulations of lunar crater degradation have been correlated to geologic units of known ages. This model provides a valuable tool in assessing the ages of geologic units, especially in the variety of maria identified on the lunar farside [*Gillis and Spudis*, 1996]. However, the reliability of this model is predicated on analyzing all degraded craters within a given unit.

From the analysis of degraded craters located in the Apollo mare deposit, this material was probably emplaced during the Imbrian. On the basis of quantitative assessments of degraded impact craters located in this deposit, a total effective thickness of <1 m of mare material was eroded and redistributed. The average lunar erosion rate since the Imbrium is estimated to be $2.0 \pm 0.1 \times 10^{-7}$ mm/yr; however, this rate appears to have decreased through the Eratosthenian and Copernican.

References

Belton, M.J.S., et al., Galileo multispectral imaging of the north polar and eastern limb regions of the Moon, *Science, 264*, 1112-1115, 1994.

Boyce, J.M., and A.L. Dial, Relative ages of flow units in Mare Imbrium and Sinus Iridum, *Proc. Lunar Planet. Sci. Conf., 6th*, 2585-2595, 1975.

Boyce, J.M., A.L. Dial, and L.A. Soderblom, A summary of relative ages of lunar nearside and farside plains, *U.S. Geol. Surv. Interagency Rep.: Astrogeology 66*, 26 pp., 1975.

Brooks, C.G., J.M. Grimwood, and L.S. Swenson Jr., *Chariots for Apollo: A History of Manned Lunar Spacecraft, NASA SP-4205*, 538 pp., Nat. Aeronaut. Space Admin., Washington, D.C., 1979.

Carr, M.H., K.A. Howard, and F. El-Baz, Geologic map of the Appennine-Hadley region of the Moon: Apollo 15 pre-mission map, *U.S. Geol. Surv. Misc. Geol. Invest. Map, I-723*, scale 1:1,000,000, 1971.

Compston, W., J.R. de Laeter, and M.J. Vernon, Strontium isotope geochemistry of Apollo 15 basalts (abstract), in *The Apollo 15 Lunar Samples*, pp. 347-351, Lunar Sci. Inst., Houston, Tex., 1972.

Craddock, R.A., Geomorphic analyses of degraded craters on the Moon and Mars, Ph.D. dissertation, Univ. of Va., Charlottesville, May 1999.

Craddock, R.A., T.A. Maxwell, and A.D. Howard, Crater morphometry and modification in the Sinus Sabaeus and Margaritifer Sinus regions of Mars, *J. Geophys. Res., 102*, 13,321-13,340, 1997.

Davis, P.A., and A.S. McEwen, Photoclinometry: Analysis of inherent errors and implications for topographic measurements (abstract), *Lunar Planet Sci.*, XV, 194-195, 1984.

Davis, P.A., and L.A. Soderblom, Modelling crater topography and albedo from monoscopic Viking orbiter images, *J. Geophys. Res., 89*, 9449-9457, 1984.

Fournier, F., *Climat et Erosion: La Relation Entre l'Erosion du Sol par l'Eau et les Precipitations Atmospheriques*, 201 pp., P.U.F., Paris, 1960.

Gault, D.E., F. Hörz, and J.B. Hartung, Effects of microcratering on the lunar surface, *Proc. Third Lunar Sci. Conf., 3*, 2713-2734, 1972.

Gillis, J.J., and P.D. Spudis, The composition and geologic setting of lunar farside maria (abstract), *Lunar Planet. Sci., XXVII*, 413-414, 1996.

Goguen, J.D., A theoretical and experimental investigation of the photometric functions of particulate surfaces, Ph.D. dissertation, Cornell Univ., Ithaca, N.Y., 1981.

Grieve, R.A.F., M.R. Dence, and P.B. Robertson, Cratering processes: As interpreted from the occurrence of impact melts, in *Impact and Explosion Cratering* (D.J. Roddy, R.O. Pepin, and R.B. Merrill, eds.), pp. 791-814, Pergamon, Tarrytown, N. Y., 1977.

Hapke, B., Bi-directional reflectance spectroscopy, 1, Theory, *J. Geophys. Res., 86*, 3039-3054, 1981.

Head, J.W., Lunar volcanism in space and time, *Rev. Geophys., 14*, 265-300, 1976.

Hörz, F., R. Grieve, G. Heiken, P. Spudis, and A. Binder, Lunar Surface Processes, in *Lunar Sourcebook: A User's Guide to the Moon*, edited by G.H. Heiken, D.T. Vaniman, and B.M. French, pp. 61-120, Cambridge Univ. Press, New York, 1991.

Howard, A.D., A detachment-limited model of drainage basin evolution, *Water Resour. Res., 30*, 2261-2285, 1994.

Howard, K.A., J.W. Head, and G.A. Swann, Geology of Hadley Rille, *Proc. Third Lunar Sci. Conf., 1*, 1-14, 1972.

Jankowski, D.G., and S.W. Squyres, Sources of error in planetary photoclinometry, *J. Geophys. Res., 96*, 20,907-20,922, 1991.

Langevin, Y., and J.R. Arnold, The evolution of the lunar regolith, *Annu. Rev. Earth Planet. Sci., 5*, 449-489, 1977.

Lucey, P.G., G.J. Taylor, and E. Malaret, Abundance and distribution of iron on the Moon, *Science, 268*, 1150-1153, 1995.

Lucey, P.G., D.T. Blewett, G.J. Taylor, and B.R. Hawke, Imaging of lunar surface maturity, *J. Geophys. Res.*, this issue.

McEwen, A.S., Photometric functions for photoclinometry and other applications, *Icarus, 92*, 298-311, 1991.

McEwen, A.S., L.R. Gaddis, G. Neukum, H. Hoffman, C.M. Pieters, and J.W. Head, Galileo observations of post-Imbrian lunar craters during the Earth-Moon flyby, *J. Geophys. Res., 98*, 17,207-17,234, 1993.

McEwen, A.S., J.M. Moore, and E.M. Shoemaker, The Phanerozoic impact cratering rate: Evidence from the farside of the Moon, *J. Geophys. Res., 102*, 9231-9242, 1997.

McGetchin, T.R., M. Settle, and J.W. Head, Radial thickness variation in crater ejecta: Implications for lunar basin models, *Earth Planet Sci. Lett., 20*, 226-236, 1973.

McKay, D.S., G. Heiken, A. Basu, G. Blanford, S. Simon, R. Reedy, B.M. French, and J. Papike, The lunar regolith, in *Lunar Sourcebook: A User's Guide to the Moon*, edited by G.H. Heiken, D.T. Vaniman, and B.M. French, pp. 285-356, Cambridge Univ. Press, New York, 1991.

Moore, H.J., J.M. Boyce, and D.A. Hahn, Small impact craters in the lunar regolith-their morphologies, relative ages, and rates of formation, *Moon and Planets, 23*, 231-252, 1980a.

Moore, H.J., J.M. Boyce, G.G. Schaber, and D.H. Scott, Lunar remote sensing and measurements, *U.S. Geol. Surv. Prof. Pap.-1046*, B1-B78, 1980b.

Neukum, G., B. König, H. Fechtig, and D. Storzer, Cratering in the Earth-Moon system: Consequences for age determination by crater counting, *Proc. Lunar Sci. Conf., 6*, 2597-2620, 1975.

Nozette, S. et al., The Clementine mission to the Moon: Scientific overview, *Science, 266*, 1835-1839, 1994.

Offield, T.W., and H.A. Pohn, Lunar crater morphology and relative-age determination of geologic units-part 2.

Applications, in *Geologic Survey Research*, *U.S. Geol. Surv. Prof. Pap. 700-C*, pp. C163-C169, 1970.

Pike, R.J., Depth/diameter relations of fresh lunar craters: Revision from spacecraft data, *Geophys. Res. Lett.*, *1*, 291-294, 1974.

Pike, R.J., Apparent depth/diameter relations for lunar craters, *Proc. Lunar Planet. Sci. Conf.*, *8*, 3427-3436, 1977.

Pohn, H.A., and T.W. Offield, Lunar crater morphology and relative-age determination of geologic units part 1, Classification, in *Geologic Survey Research*, *U.S. Geol. Surv. Prof. Pap. 700-C*, C153-C162, 1970.

Ryder, G., D. Bogard, and D. Garrison, Probable age of Autolycus and calibration of lunar stratigraphy, *Geology*, *19*, 143-146, 1991.

Settle., M., J.W. Head, and T.R. McGetchin, Ejecta from large craters on the Moon: Discussion, *Earth and Planet. Sci. Lett.*, *23*, 271-274, 1974.

Smith, E.I., and A.G. Sanchez, Fresh lunar craters: Morphology as a function of diameter, a possible criterion for crater origin, *Mod. Geol.*, *4*, 51-59, 1973.

Soderblom, L.A., The distribution and ages of regional lithologies in the lunar maria, Ph.D. dissertation, Dept. of Geol. Sci., Calif. Inst. of Technol., Pasadena, 1970a.

Soderblom, L.A., A model for small-impact erosion applied to the lunar surface, *J. Geophys. Res.*, *75*, 2655-2661, 1970b.

Soderblom, L.A., and L.A. Lebofsky, Technique for rapid determination of relative ages of lunar areas from orbital photography, *J. Geophys. Res.*, *77*, 279-296, 1972.

Swann, G.A., et al., 5. Preliminary geologic investigation of the Apollo 15 landing site, in *Apollo 15 Preliminary Science Report*, *NASA SP-289*, pp. 5-1 to 5-112, Nat. Aeronaut. Space Admin., Washington, D.C., 1972.

Taylor, S.R., *Planetary Science: A Lunar Perspective*, 481 pp., Lunar and Planet. Inst., Houston, Tex., 1982.

Trask, N.J., Geologic maps of the early Apollo landing sites, explanatory pamphlet accompanying *U.S. Geol. Surv. Maps I-616 through I-627*, 4 pp., 1969.

Trask, N.J., Geologic comparison of mare materials in the lunar equatorial belt, including Apollo 11 and Apollo 12 landing sites, in *Geological Survey Research*, *U.S. Geol. Surv. Prof. Pap. 750-D*, D138-D144, 1971.

Weissman, P.R., Terrestrial impact crater rates for long and short period comets, *Spec. Pap. Geol. Soc. Am.*, *190*, 15-24, 1990.

Wilhelms, D.E., The Moon, in *The Geology of the Terrestrial Planets*, edited by M.H. Carr et al., pp. 107-205, *NASA SP-469*, Natl. Aeronaut. Space Admin., Washington, D.C., 1984.

Wilhelms, D.E., The geologic history of the Moon, *U.S. Geol. Surv. Prof. Pap. 1348*, 302 pp., 1987.

Wilhelms, D.E., *To a Rocky Moon: A Geologist's History of Lunar Exploration*, 477 pp., Univ. of Ariz. Press, Tucson, 1993.

Wilhelms, D.E., and J.F. McCauley, Geologic map of the near side of the Moon, *U.S. Geol. Surv. Misc. Invest. Ser. Map, I-703*, scale 1:5,000,000, 1971.

Wilhelms, D.E., V.R. Oberbeck, and H.R. Aggarwal, Size-frequency distributions of primary and secondary lunar impact craters, *Proc. Lunar Planet. Sci.*, *9*, 3735-3762, 1978.

Zuber, M.T., D.E. Smith, F.G. Lemoine, G.A. Neumann, The shape and internal structure of the Moon from the Clementine mission, *Science*, *266*, 1839-1843, 1994.

R.A. Craddock, Center for Earth and Planetary Studies, National Air and Space Museum, Smithsonian Institution, Room 3776, MRC-315, Washington, DC 20560. (craddock@ceps.nasm.edu)

A.D. Howard, Department of Environmental Sciences, University of Virginia, Charlottesville, VA 22903. (ah6p@virginia.edu)